Ultrasonics Sonochemistry 76 (2021) 105633

Contents lists available at ScienceDirect

Ultrasonics Sonochemistry

journal homepage: www.elsevier.com/locate/ultson

Wetting of aluminium and carbon interface during preparation of Al-Ti-C grain refiner under ultrasonic field

Jingtao Zhao [a,b], Xiaoyu Wu [a,b], Liping Ning [a,b], Junjia Zhang [a,b], Chao Han [c], Yinglong Li [a,b,*]

[a] School of Materials Science and Engineering, Northeastern University, 11 Wenhua Road, Shenyang 110819, PR China
[b] Key Laboratory of Lightweight Structural Materials, Liaoning Province, PR China
[c] School of Metallurgy, Northeastern University, Shenyang 110819, PR China

ARTICLE INFO

Keywords:
Ultrasonic field
Wetting
Interface
TiC

ABSTRACT

In the preparation of an Al-Ti-C grain refiner under an ultrasonic field, the mechanism of the wetting behaviour between Al and C was systematically investigated. The results demonstrated that the wetting behaviour was mainly dependent on the wetting of the Al melt on graphite under the ultrasonic field (physical wetting) and the formation and mass transfer of TiC (reactive wetting). The diffusion of Ti atoms and their adsorption around the graphite could contribute to the wetting of Al-C. TiC particles were formed under the high temperature caused by the cavitation effect, and they detached from the interface due to the sound pressure, which resulted in consistently sufficient contact on the wetting interface. Moreover, the wetting and spreading behaviour of the Al melt on graphite under an ultrasonic field were numerically simulated, strongly manifesting that the ultrasonic field could facilitate the wetting of the Al-C interface.

1. Introduction

Al alloys are widely used in several industries, such as oil, gas, transport, and aerospace, because of their low density, high strength, and stable service performance. Grain refinement is a key technical step in the production of Al alloys, and it could significantly affect the properties and application range of the material [1–5]. The most common contemporary methods for grain refinement include the adoption of physical fields and the addition of grain refiners [6–8]. The adoption of a physical field, such as an electromagnetic field and an ultrasonic field, could offer excellent refinement effects [9], while the addition of grain refiners is more economical and effective. Commonly used grain refiners are mainly classified into two types, Al-Ti-C and Al-Ti-B [10–13]. Compared with Al-Ti-C, Al-Ti-B has many disadvantages. Al-Ti-B grain refiners are not suitable for molten Al alloys containing Cr, Mn, Zr, and V, as the B causes “poisoning”, and the refining activity is impeded by the precipitation of TiB_2 [14–17]. In the last few decades, Al-Ti-C grain refiners have been extensively studied by researchers and utilised in industrial applications, since they could overcome the disadvantages of Al-Ti-B grain refiners [18]. During the solidification process, because of the soluble second phase Al_3Ti in the Al-Ti-C refiner, the TiC particle acts as a heterogeneous nucleation site for primary α-Al, resulting in the good grain refinement for Al alloys [1,19,20]. Vinod et al. [21,22] found that in the Al-Ti-C refiner, compared with TiB_2, the improvement in the nucleation rate by the TiC particles is better. However, the preparation of Al-Ti-C grain refiners is difficult, due to the poor wetting of the Al-C interface [23,24].

To improve the wetting of the Al-C interface during the preparation of Al-Ti-C grain refiners, researchers have employed a series of strategies such as strong mechanical agitation and the addition of rare earth elements [2,25]. However, these methods also possess great disadvantages, such as the complicated production process requirements and high production costs. Recent studies show that the ultrasonic treatment in melt processing can improve the preparation and processing environment of materials, bringing about a better microstructure and improved properties [26–33]. Ultrasonic fields have acoustic cavitation and acoustic streaming effects [34–36], which can reduce the interface energy between the particle and the melt, and thus activate the impurities to act as effective nucleation substrates. In addition, ultrasonic fields can promote particle movement and improve particle dispersion [37]. The application of an ultrasonic field in the preparation of Al-Ti-C refiners was shown to induce the homogenous distribution of the second phase Al_3Ti and the particle phase TiC in the matrix, thus enhancing the refinement effect [38]. Eskin et al. [37,39] reported that the ultrasonic

* Corresponding author at: School of Materials Science and Engineering, Northeastern University, 11 Wenhua Road, Shenyang 110819, PR China.
E-mail address: liyl@smm.neu.edu.cn (Y. Li).

https://doi.org/10.1016/j.ultsonch.2021.105633
Received 3 May 2020; Received in revised form 25 May 2021; Accepted 14 June 2021
Available online 18 June 2021

Table 1
Chemical composition of the industrial pure Al (wt.%).

Fe	C	Si	Zn	Ga	S	Al
0.1153	0.0823	0.1140	0.0225	0.0178	0.0027	Bal.

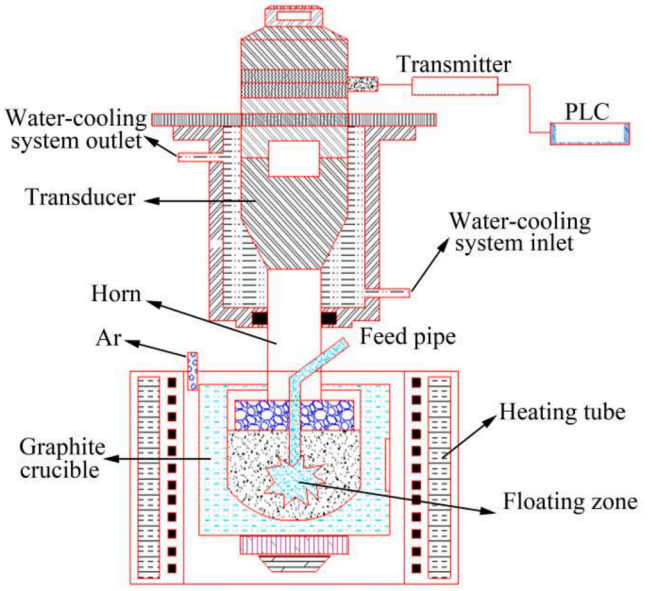

Fig. 1. Schematic diagram of the reaction system for preparing Al-Ti-C grain refiner under ultrasonic field.

field facilitates the wetting of particles with the Al melt and involves the reinforced phase and particle phase as nuclei during solidification. Ultrasonic fields have been successfully employed in the preparation of Al_2O_3 and TiC particulate reinforced Al matrix composite materials [40,41]. These studies demonstrate that high intensity ultrasonic fields can enhance melt infiltration and particulate dispersion in a very short time and improve the wetting between the reinforced phase and the molten matrix [42].

However, few studies have investigated the Al-C wetting behaviour during the preparation of Al-Ti-C grain refiners under an ultrasonic field. In this study, a 20 kHz ultrasonic transmitter was employed in the in situ preparation of Al-5Ti-0.25C grain refiners. The wetting behaviour and mass transfer on the Al-C interface, as well as the formation mechanism of Al_3Ti and TiC, were systematically analysed.

2. Experimental

2.1. Materials and methods

Al-5Ti-0.25C grain refiners were prepared by melting industrial pure Al (99.65 wt%, Beijing Zhongjinyan New Material Technology Co., Ltd, China), potassium fluorotitanate (K_2TiF_6, 99.5 wt%, Shanghai Macklin Biochemical Technology Co., Ltd, China) and graphite powder (99.95 wt %, Shanghai Macklin Biochemical Technology Co., Ltd, China) in a graphite crucible with an inner diameter of 40 mm and a height of 30 mm [43]. Table 1 shows the chemical composition of the industrial pure Al; the particle size of the experimental graphite powder is 8000 mesh.

The preparation device for the Al-Ti-C grain refiners comprised an ultrasonic transmitter system (JY-R203G, Suzhou Sonic Ultrasonic Technology Co., Ltd, China), transducer system (USMY-150N25S, Zhangjiagang Jinfangyuan electromechanical instrument factory, China), PLC control system, water-cooling system, and argon protection system. Its schematic diagram is shown in Fig. 1. High-frequency voltage was obtained using the alternating current (AC) amplifier in the transmitter, and the electrical energy was converted into mechanical energy through the telescopic electronic chip in the transducer to cause high-frequency oscillations. Finally, through an ultrasonic horn, a high intensity ultrasonic field with a magnifying amplitude was applied on the metal melt. The horn was made of special niobium alloy, which can withstand high temperature at 1000℃. When the ultrasonic equipment was working, the transducer needs to keep the best working condition to output the efficient acoustic energy. The heat generated by the melt was transferred from the horn to the transducer, which results in the high temperature of the transducer and affects its working efficiency. To ensure the best working conditions, the transducer was cooled using circulating water to eliminate the resonance frequency drift caused by temperature fluctuation. In this study, the output power of the ultrasonic transmitter was continuously adjusted between 0 and 2 kW, and the ultrasonic frequency was 20 kHz.

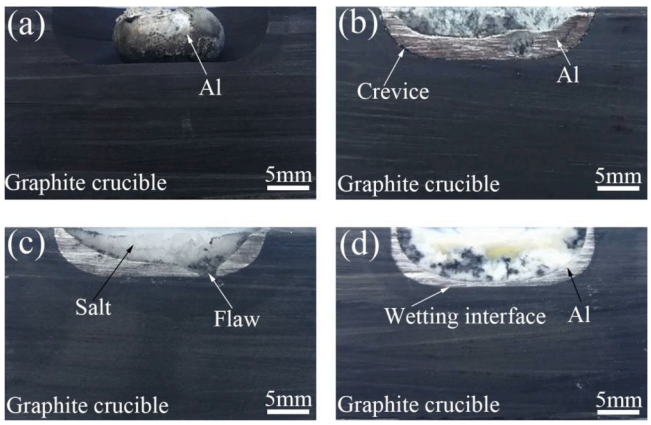

Fig. 2. The macrographs of Al-C wetting (a) sample S_O, (b)-(c) sample S_K, (d) sample S_U.

The raw materials (Al, K_2TiF_6 and graphite powder) were weighed according to the element mass percentage of Al-5Ti-0.25C, and then, the K_2TiF_6 powder and graphite powder were mixed in a ball mill for 3 h. Pure Al was heated in the crucible to 1000 °C under a high purity argon atmosphere to avoid the potential reaction between air and the graphite powder. The mixed powders were then added to Al through a feed pipe, and the entire mixture was mechanically stirred using a Ti rod. The ultrasonic field was applied to the melt for 5, 10, 15, 20, and 30 min, to analyse its effect on the Al-C wetting behaviour, and the obtained sample was denoted as S_U. For comparison, the grain refiner was also prepared (1) without K_2TiF_6 and ultrasonic treatment (denoted as S_O) and (2) with K_2TiF_6 but without ultrasonic treatment (denoted as S_K).

2.2. Microstructure and property

The microstructures of the samples were observed using an Olympus DSX500 optical digital microscope and a Zeiss Supra 55 scanning electron microscope (SEM) equipped with energy dispersive spectroscopy (EDS). The samples were placed in a boron nitride crucible under argon and air, respectively, and then heated from 400 to 1100 °C at 20 °C/min in a STA449F3 synchronous thermal analyser for the differential scanning calorimetry (DSC) analysis [44].

3. Results

3.1. Wetting phenomenon

The wetting results under the equilibrium condition are shown in Fig. 2. The contact angle (denoted as θ) of the Al-C system without K_2TiF_6 and ultrasonic treatment is approximately 130° in S_O, which is in agreement with previous data [45,46]. The Al melt is solidified in a spherical shape at the bottom of the graphite crucible [43], as shown in

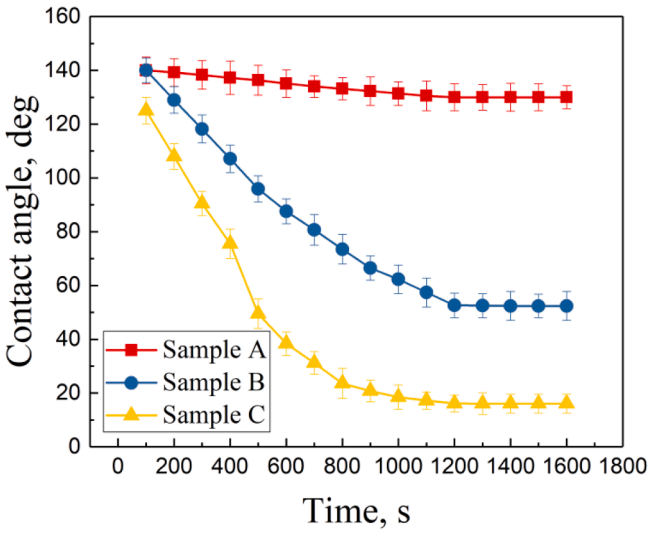

Fig. 3. The change curve of contact angle of Al-C system with different time.

Fig. 2a. With the addition of the K_2TiF_6 salt, S_K displays better wetting behavior, which is demonstrated by the spreading of the Al melt on the bottom of the crucible, as shown in Fig. 2b and c. However, numerous obvious crevices and pore flaws are observed at the Al-C interface. It should be mentioned that the Al droplet was able to climb up along the crucible wall only till the top of the salt layer [47]. These defects are not easily observed in S_U, indicating the occurrence of complete wetting, which is obtained by adding the K_2TiF_6 salt and employing the ultrasonic treatment, as shown in Fig. 2d.

To describe the wetting results more accurately, the θ of the Al-C system was determined, as displayed in Fig. 3. Due to the oxide film that formed on the Al surface [46–48], the θ of S_O remains stable from 130° to 140°, signifying poor wetting between Al-C. With the addition of the K_2TiF_6 salt, the θ of S_K decreases significantly from 140° to 52°. When an ultrasonic field is also applied to the flux-assisted Al-C system (S_U), the θ changes more rapidly, from 125° to 16°. Compared with S_O and S_K, S_U has a smaller initial and transient θ, which can be attributed to the presence of sound pressure; the decrease in surface tension resulting from the ultrasonic treatment promotes the rapid spread of Al droplets on graphite. In addition, the active Ti ions ionised by the K_2TiF_6 salt are adsorbed onto the surface of graphite, which enhances the wetting behaviour between Al-C.

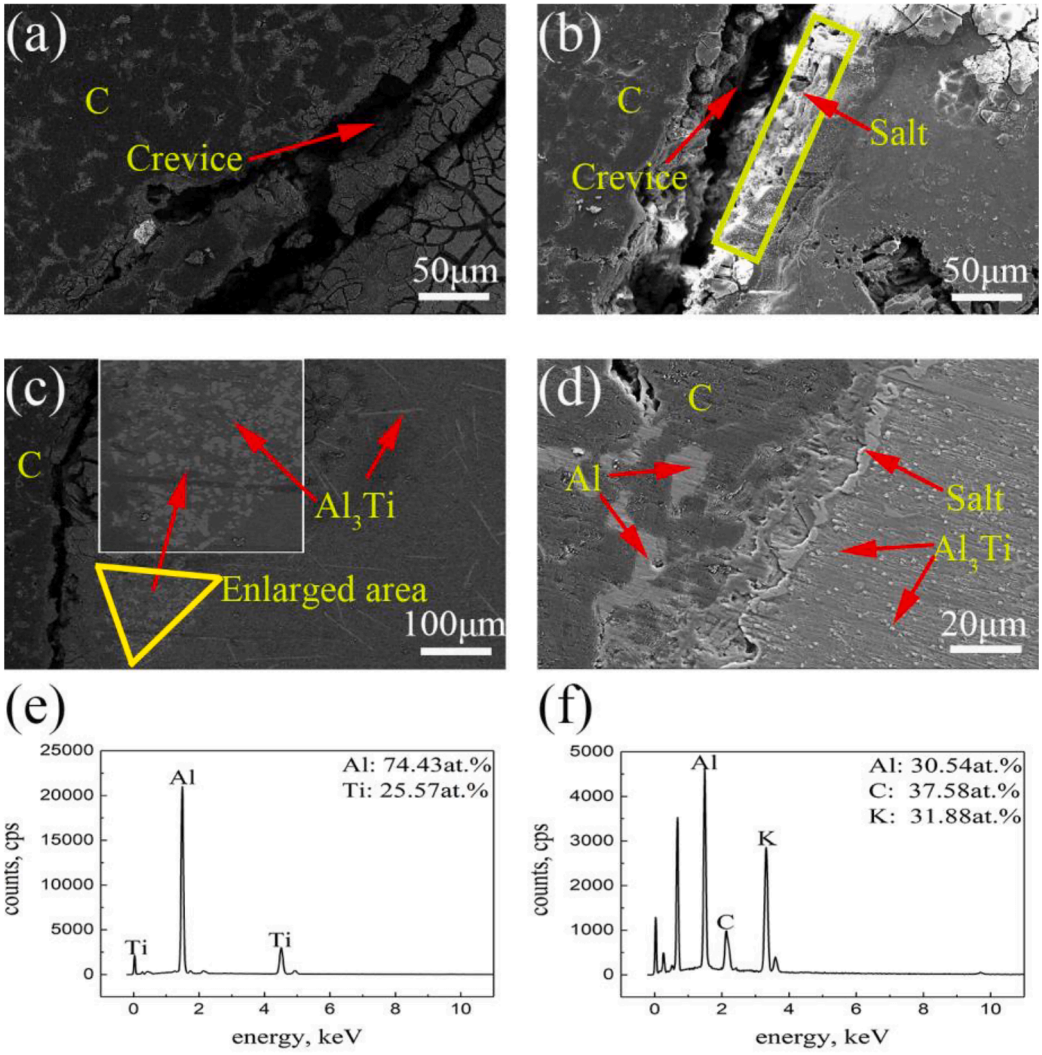

Fig. 4. The SEM of Al-C wetting interface (a) sample S_O, (b)-(c) sample S_K, (d) sample S_U, (e) the EDS point analysis of chemical composition for Al_3Ti in S_K, (f) the EDS point analysis of chemical composition for Al in S_U.

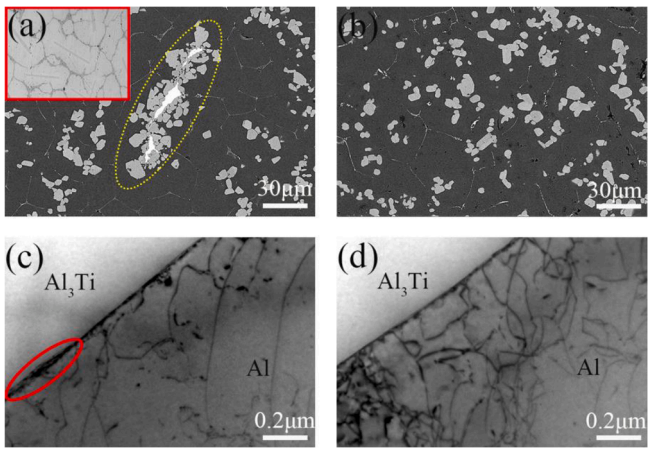

Fig. 5. The micrographs of the Al-5Ti-0.25C grain refiner (a) the SEM of the S_K sample, (b) the SEM of the S_U sample, (c) the TEM of the S_K sample, (d) the TEM of the S_U sample.

3.2. Interfacial structure

The microstructure of the Al-C interface is shown in Fig. 4. There was an obvious crack at the Al-C interface in S_O, which was fabricated without any additional external conditions. Fig. 4b and c show the higher magnification micrograph of the crevice region in Fig. 2c. A salt layer can be observed between the crevice and the Al matrix (Fig. 4b), and numerous Al_3Ti phases are detected in the interfacial region. As shown in Fig. 4c, these Al_3Ti phases mainly exist in two forms: the block-like Al_3Ti near the interface and the needle-like Al_3Ti far from the interface. Once added into the Al melt, the Ti salts mainly aggregate at the Al-C interface and cause a violent Al-Ti exothermal reaction. In this case, this leads to a local high temperature that melts the needle-like Al_3Ti, which ultimately forms the block-like Al_3Ti. As the holding time increases and the reaction progresses, the Ti atoms continuously diffuse into the melt. When they precipitate again from the supersaturated melt in the form of Al_3Ti, the growth rate in the [0 0 1] direction is low, which significantly increases the preferential growth trend and eventually causes the formation of needle-like Al_3Ti far from the interface. The acoustic streaming effect of ultrasonic field can accelerate the diffusion of Ti near the interface into the Al melt, which is beneficial to distribute Ti uniformly in the melt and improve the reaction rate of the Ti ions with Al. Simultaneously, the local instantaneous high temperature in the melt caused by the acoustic cavitation makes the needle-like Al_3Ti break. As a result, more Al_3Ti uniformly distributed phases are generated in the block-like form, as shown in Fig. 4d. The phenomenon of Al_3Ti as a block-like after ultrasonic treatment was consistent with the mechanism that cavitation bubbles break the growing solid dendrites or particles reported by Eskin et al. [38,49,50]. The typical chemical bond morphology of the Al-C interface layer is also observed in Fig. 4d. Fig. 4e shows the EDS analysis results of the Al_3Ti phase in Fig. 4c and d, and Fig. 4f shows the EDS analysis results of Al in Fig. 4d.

In the absence of ultrasonic field, the block-like Al_3Ti phase (yellow dotted line) is mainly concentrated in the grain boundaries (GBs) and grain interior of α-Al grains, while the needle-like Al_3Ti phases (red region) is only formed in the GBs, as shown in Fig. 5a. The block-like Al_3Ti phases covers about 50% of the GBs, where it forms continuous layers with a mean thickness of 20 μm. After ultrasonic treatment, the continuous block-like Al_3Ti phases on the GBs is disappeared and evenly distributed in the grain interior. Moreover, only a very small amount of block-like Al_3Ti is covered on GBs, about 5% of the GBs, as shown in Fig. 5b. The reason for the change of the Al_3Ti particles is that the ultrasonic field increases the temperature of the liquid phases near the Al_3Ti interface and reduces the surface tension, which improves the wetting between the liquid phase and Al_3Ti particles [42]. Another

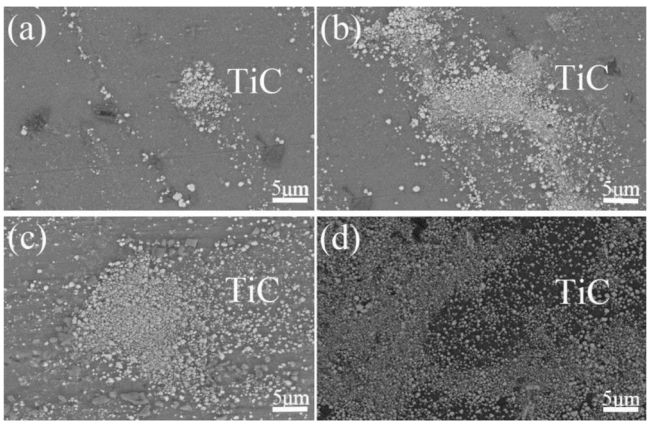

Fig. 6. The SEM micrographs of TiC (a) without ultrasonic, (b) ultrasonic 10 min, (c) ultrasonic 20 min, (d) ultrasonic 30 min.

important reason is that the Al_3Ti and α-Al have a high degree of lattice matching, and α-Al solidifies and grows with Al_3Ti as the nucleation point, which resulting a grain morphology of α-Al wrapped Al_3Ti (Fig. 5b) in the final. The difference to the fraction of covered GBs between S_U sample and S_K sample confirms the existence of the solid phase GB wetting transition in the Al-Ti-C grain refiner [51]. Similar phenomenon of GBs completely and/or incompletely covered with layers of a second solid phase have been observed also in Al alloys, Cu alloys and Ti alloys et al. [52–55]. The microstructure after ultrasonic treatment reveals significant difference from the initial state. The shape of the second phase Al_3Ti has changed, and all the needle-like Al_3Ti disappeared and become block-like, which is similar to the shape change of the second phase after heat treatment in the Mg-alloy EZ33A described in Ref [51]. Fig. 5c shows the TEM image of the interface between the Al matrix and Al_3Ti in the U_K sample, the interface of the red area, which indicated that the interface bonding was poor. The microstructure after ultrasonic treatment can be clearly seen that the phase interface of Al matrix and Al_3Ti is tightly bonded and there is no reactant transition layer, as shown in Fig. 5d. The observed effects are based on the fact that the ultrasonic field promotes the wetting of Al_3Ti particles and Al matrix. The application of an ultrasonic field significantly refines the grain size and increases the dislocation density (Fig. 5d), which can improve the strength-ductility match in materials [56].

The distribution of TiC particles is shown in Fig. 6, in which the white granular region relating to the TiC phases has an average diameter of 0.5 μm. There is a small amount of TiC particles in the matrix (Fig. 6a), and this amount is significantly increased by the application of an ultrasonic field for 10 min (Fig. 6b). With 20 min of ultrasonic treatment, the TiC particles begin to show a dispersed distribution, as shown in Fig. 6c, and this dispersed distribution is achieved for all particles after 30 min of ultrasonic treatment (Fig. 6d). This may be due to two factors: first, ultrasonic energy enables carbon particles to obtain energy, which can remove the gas impurities adsorbed by carbon powder and improve the surface activity of the carbon particles [41,42], thereby accelerating the Ti-C reaction to increase the amount of TiC; second, ultrasonic vibration promotes the movement of TiC, resulting in a dispersed distribution [37,38,42]. In conclusion, Al_3Ti and TiC are generated at the Al-C interface, as shown in Fig. 5 and Fig. 6, which ultimately leads to excellent reactivity and wetting between the Al melt and graphite.

Fig. 7 shows the SEM-EDS line scan analysis of S_U. As shown in Fig. 7a, a large amount of Al is observed in the C layer, which indicates that the ultrasonic field promotes the diffusion of the Al melt into the C layer to achieve wetting. A small amount of Ti is also detected in the C layer, and it is evenly distributed throughout the detected region. Fig. 7b indicates that the segregation region of the particle phase is rich in Ti and C and poor in Al. This is because the free Ti atoms in the Al melt preferentially surrounds the graphite particles, generating TiC.

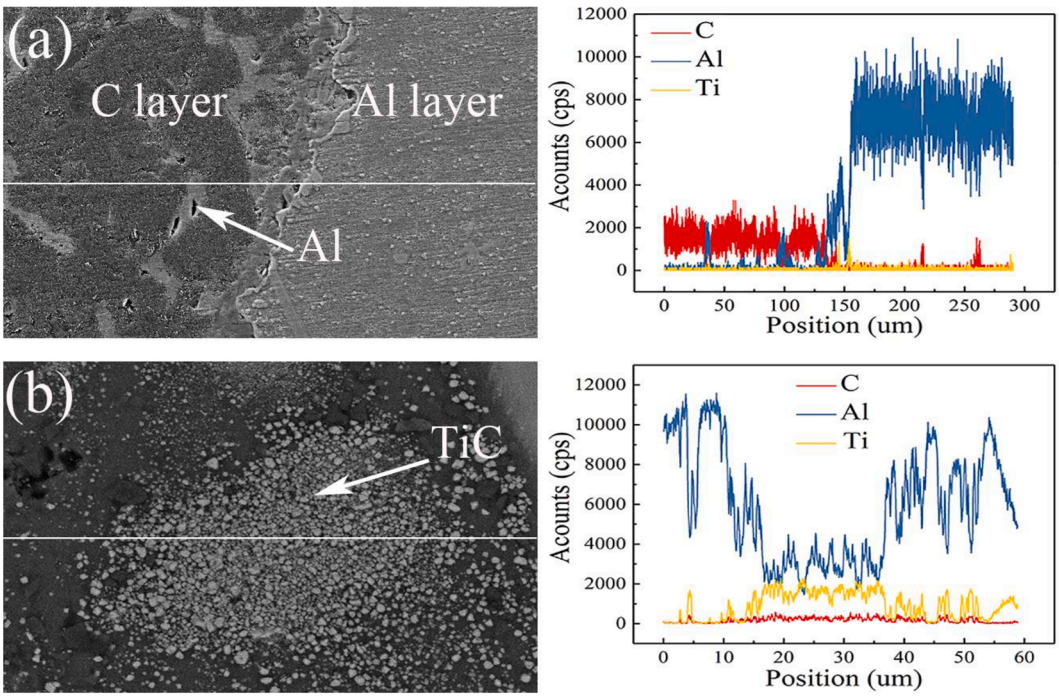

Fig. 7. SEM-EDS line scan analysis of S_U under ultrasonic field (a) SEM image (line scan region of Al-C interface) and EDS spectrum, (b) SEM image (line scan region of TiC) and EDS spectrum.

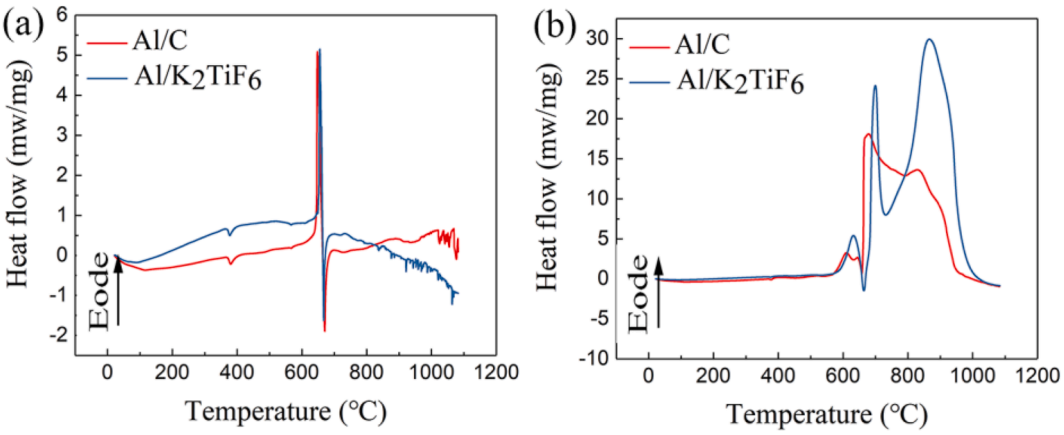

Fig. 8. DSC curves for the binary mixed powder (a) under air, (b) under argon.

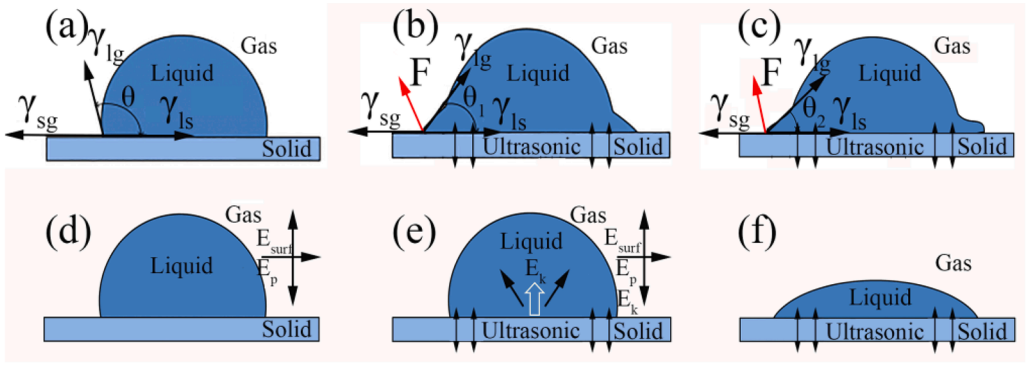

Fig. 9. The diagram of spreading wetting of Al melt on graphite is analyzed from the perspective of dynamic and energy (a)-(c) the perspective of dynamics, (d)-(f) the perspective of energy.

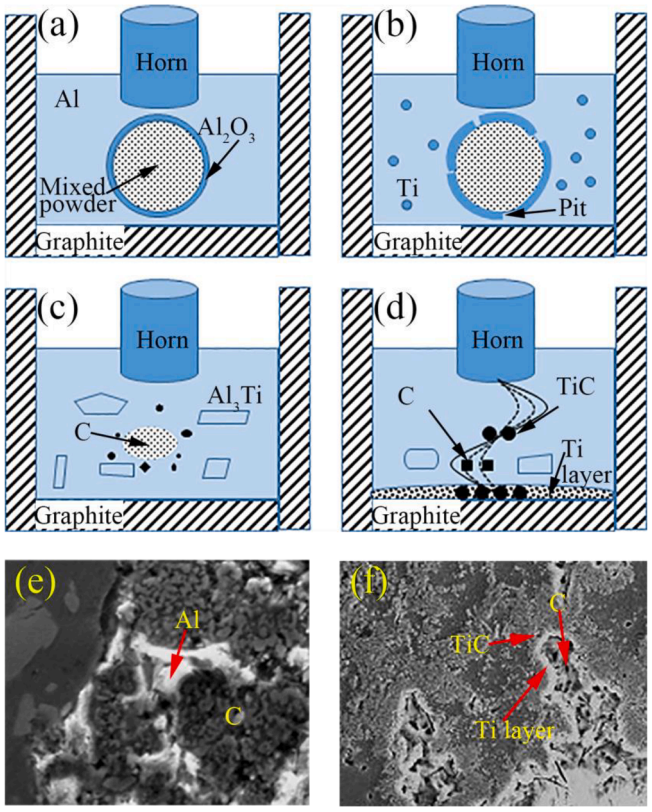

Fig. 10. The schematic diagrams and SEM of Al-C reactive wetting (a) without ultrasonic, (b)-(d) ultrasonic was performed for 5min, 15min and 30min, respectively, (e)-(f) the SEM of the Al-C interface of (c) and (d), respectively.

Fig. 8 shows the DSC curves for the binary mixed powder under air (Fig. 8a) and argon (Fig. 8b) atmospheres. For the Al-C couple, an obvious endothermic peak corresponding to Al melting is observed at 670 °C under both air and argon atmospheres. There is an exothermic peak at 400 °C, signifying the slow oxidation of the C powder under the air atmosphere. This reaction is significantly accelerated at 1000 °C, resulting in the continuous exothermic peaks, as shown in Fig. 8a. Under argon atmosphere, the K_2TiF_6 decomposes at 710 °C, and the thermite reaction occurs at 900 °C. The generated amount of Al_3Ti from the Al_4C_3 formation in the Al-C reaction under air is less than that under argon, resulting in the decomposed peak of K_2TiF_6 and the almost overlapping peak of the Al melt.

4. Discussion

4.1. Wetting mechanism

4.1.1. Physical wetting

Analysed from the perspective of dynamics and energy, the diagram of the wetting behaviour of the Al melt on graphite is shown in Fig. 9. Specifically, the original θ under an equilibrium surface tensions is an obtuse angle (Fig. 9a), and the periodic force (F) caused by the ultrasonic field changes it to an acute angle θ_1 (Fig. 9b), indicating better wetting. Fig. 9c shows that θ_2 continues to decrease ($\theta_1 > \theta_2$) as the next F is generated, and F is gradually applied to further reduce θ_2 to achieve better wetting. Fig. 9d to f show the diagram of the Al-C wetting process in terms of energy, and the Al melt wetting and spreading on the graphite surface can be attributed to the transition from the gravitational potential energy (represented by E_P) to the surface energy (represented by E_{surf}). Fig. 9d shows that the decrease in the gravity potential energy of the Al melt increases the surface energy and impedes the spreading behaviour. The additional molecular kinetic energy

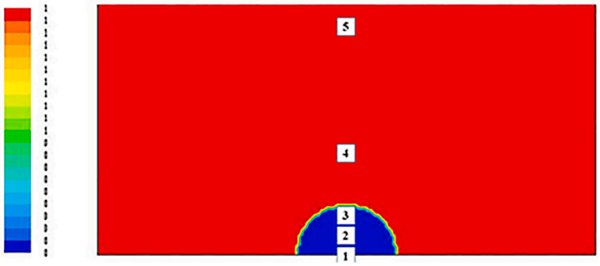

Fig. 11. The positions of the five selected points in the gas–liquid phase diagram at the initial moment.

(represented by E_K) resulting from the applied ultrasonic field enhances the kinetic energy of the liquid molecules as they come in contact with the gas–liquid interface, as shown in Fig. 9e. When the summation of E_K and E_P is greater than the increase in E_{surf}, the wetting and spreading occur spontaneously (Fig. 9f), due to the lowest energy principle.

4.1.2. Reactive wetting

Since the high surface tension of the oxide film, wetting behaviour cannot occur at the interface between the mixed powder and the melt, as shown in Fig. 10a. The instantaneous high temperature and high pressure caused by the applied ultrasonic cavitation for 5 min simultaneously breaks up the oxide film and forms a pit (Fig. 10b) [50], which promotes the release of free Ti ions from K_2TiF_6. Thereafter, the oxide film is entirely broken, and the Al melt reacts with the free Ti ions to directly form Al_3Ti, as shown in Fig. 10c. The Al melt infiltrates into the graphite powder through capillary action and wets the Al-C interface due to the effect of the high temperature of cavitation. At the high temperature, the Al_3Ti diffuses into the bottom of the graphite crucible and then releases Ti ions in the ultrasonic field; in this case, a Ti-rich layer, would be formed, and then TiC particles are generated at the boundary due to the reaction of the Ti ions with C. Because the direction of acoustic radiation force is related to the acoustic contrast factor of liquid medium and particles [57]. When the acoustic contrast factor is positive, the acoustic radiation force points to the sound pressure node, and the particles dispersed in the liquid medium will move to the sound pressure node under the action of the standing wave field. On the contrary, when the acoustic contrast factor is negative, the particles move to the sound pressure antinode. TiC particles move towards the sound pressure node, as their acoustic contrast factor is more than 0, while the C atoms, having an acoustic contrast factor of less than 0, move towards

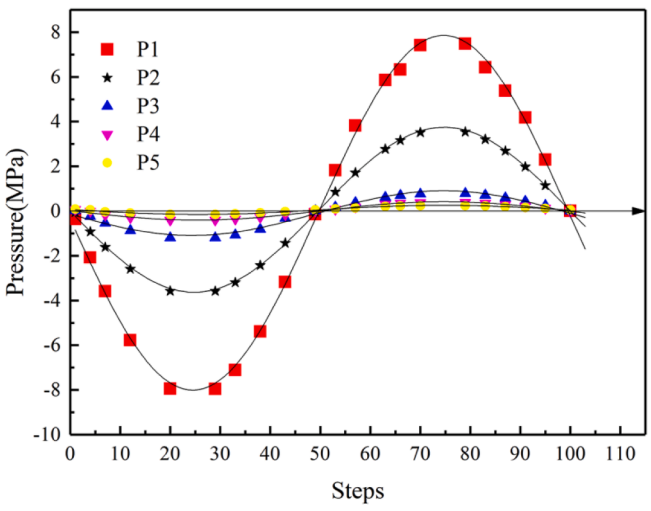

Fig. 12. The fitting curve of the pressure change at these five points in one period.

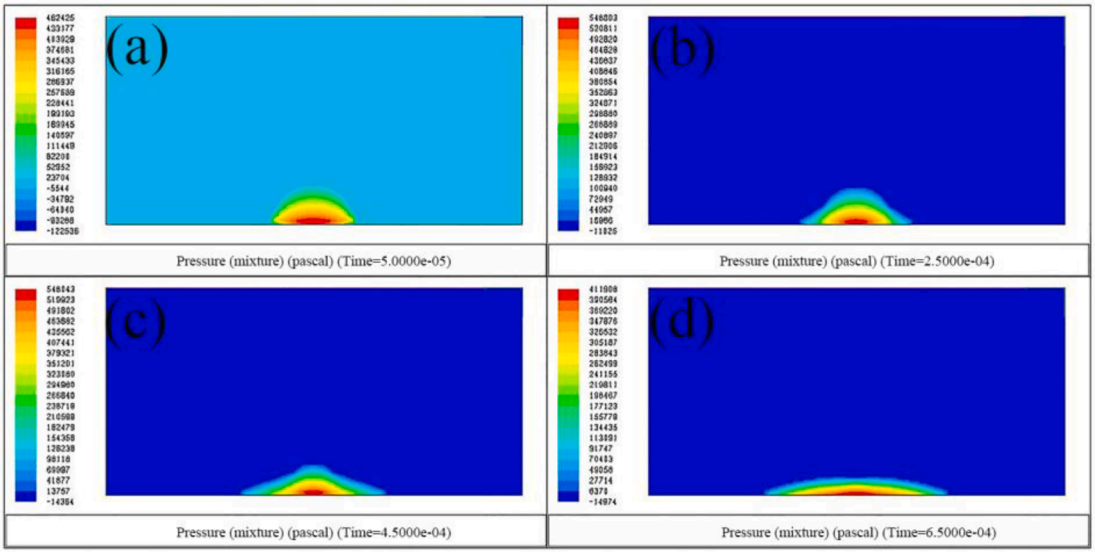

Fig. 13. The pressure of gas–liquid phases in different period under ultrasonic field (a) 1 T, (b) 5 T, (c) 9 T (d) 13 T.

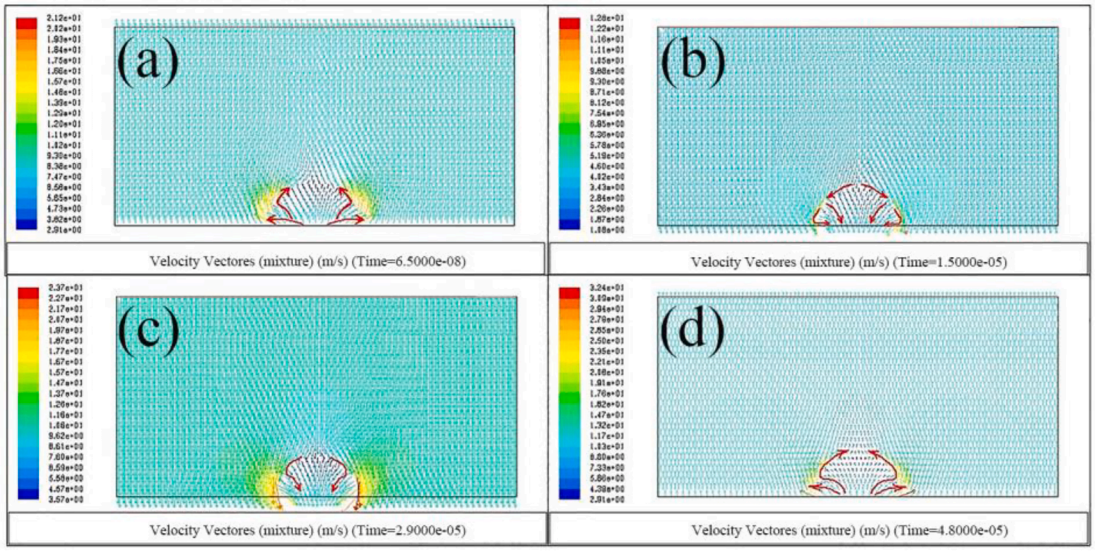

Fig. 14. The velocity vector diagram of the Al melt in one period.

the sound pressure antinode [57,58], as shown in Fig. 10d. Juhasz [43] reported the wetting of graphite by liquid Al under molten potassium halide fluxes, as shown in Fig. 10a to d; however, they did not further investigate the wetting of the Al-C interface under an ultrasonic field. Fig. 10e shows a compact Al-C interface, which indicates that the Al melt can infiltrate into the graphite powder through capillary action due to the excellent wetting. Whereas, no Al_4C_3 is formed at the Al-C interface. A large amount of active Ti atoms are dispersed and adsorbed around the graphite, which facilitates the wetting, as shown in Fig. 10f. Qiaoli Lin [59] reported that Ti atoms can improve the wetting of the liquid–solid interface. Simultaneously, it provides a favourable interfacial condition for the synthesis of TiC. The obtained TiC moves away from the carbon interface with the ultrasonic standing wave to achieve favourable reactive wetting behaviour and mass transfer.

4.2. Numerical simulation

To verify the rationality of the experiment, the wetting and spreading behaviours of the Al melt on graphite under an ultrasonic field were numerically simulated. The parameter settings were f = 20 kHz and T = 50 μs. Fig. 11 shows the positions of the five selected points in the gas–liquid phase diagram at the initial moment; the fitting curves of the pressure change at these five points in one period are shown in Fig. 12. The results demonstrate that the gas–liquid pressure changes continuously according to the simple harmonic motion, which has the same phase as that of the ultrasonic field. In addition, the pressure of each point is fairly different, and the pressure at each point in the next period will repeat the previous period, which means the pressure of each point changes periodically. Fig. 13 shows the pressure of the gas–liquid phases in different periods under an ultrasonic field. There is a certain sound pressure gradient in the melt [58,60], which eventually leads to the smooth wetting and spreading of the Al melt on the graphite. Fig. 14 is the velocity vector diagram of the Al melt in one period, and the movement of the Al melt under the ultrasonic field can be described as follows: when the system is in the pressure decreasing stage, which is steps 0–20 and 80–100 in Fig. 12, the melt flows from the centre of the bottom to the surface, as shown in Fig. 14a and d, and this movement drives melt spreading; when the system is in the pressure increasing

stage, which is steps 20–80 in Fig. 12, the mass point flows from the melt top to the melt bottom periphery, as shown in Fig. 14b and c. Due to the obstruction of the bottom boundary and surface tension, some mass point turns to the melt bottom centre, resulting in the formation of a tiny vortex at the melt inner edge. The tendency of mass point to spread from top to bottom decreases the melt height as well as θ. Meanwhile, the tiny vortex generates a centrifugal force to extend the melt boundary at all sides; in this case, the contact area between the melt and the bottom surface would increase, which is conducive for spreading. The numerical simulation results are consistent with the analytical conclusion in Fig. 9.

5. Conclusions

1) Compared with the addition of K_2TiF_6 salt, the problem of the Al-C interface wetting is solved by the application of ultrasonic field in the preparation of Al-Ti-C grain refiner. In addition, the wetting of the Al-C interface consists of physical wetting and reactive wetting. Physical wetting is the precondition of the interface reaction, and reactive wetting is the dynamic element of the sustained interface reaction.
2) The physical wetting analysis of the Al-C interface shows that the ultrasonic field offers an additional periodic force to destroy the oxide film, reduce the surface tension of the Al melt, and provide additional molecular kinetic energy to decrease the contact angle of Al-C. Meanwhile, the wetting and spreading behaviours of the Al melt on graphite under an ultrasonic field were numerically simulated, which proved that the ultrasonic field facilitated the wetting of the Al-C interface.
3) The reactive wetting analysis of the Al-C interface shows that the acoustic streaming effect promotes the Al_3Ti towards the interface, and a large amount of active Ti atoms are dispersed and adsorbed around the graphite. Simultaneously, TiC particles were formed under the high temperature caused by the cavitation effect, and they detached from the interface due to the sound pressure, which resulted in consistently sufficient contact on the Al-C interface to achieve perfect wetting.

Declaration of Competing Interest

The authors declare that they have no known competing financial interests or personal relationships that could have appeared to influence the work reported in this paper.

Acknowledgements

The authors acknowledge the project support from the Experimental methods and techniques for the behavior of solid/liquid aluminum interface under ultrasonic field coupling. Special thanks are due to the instrumental/date analysis from Analytical and Testing Center, Northeastern University.

Funding sources

This work was supported by the National Nature Science Foundation of China [grant numbers 11574043].

Appendix A. Supplementary data

Supplementary data to this article can be found online at https://doi.org/10.1016/j.ultsonch.2021.105633.

References

[1] T. Wang, T. Gao, J.F. Nie, P.T. Li, X.F. Liu, Influence of carbon source on the microstructure of Al–Ti–C master alloy and its grain refining efficiency, Mater. Charact. 83 (2013) 13–20, https://doi.org/10.1016/j.matchar.2013.06.002.
[2] W.W. Ding, C. Xu, X.G. Hou, X.Y. Zhao, T.L. Chen, W.J. Zhao, T.D. Xia, J.S. Qiao, Preparation and synthesis thermokinetics of novel Al-Ti-C-La composite master alloys, J. Alloys Compd. 776 (2019) 904–911, https://doi.org/10.1016/j.jallcom.2018.10.241.
[3] X.W. Li, Q.Z. Cai, B.Y. Zhao, B. Li, B. Liu, W.L. Ma, Grain refining mechanism in pure aluminum with nanosized TiN/Ti composite refiner addition, J. Alloys. Compd. 699 (2017) 283–290, https://doi.org/10.1016/j.jallcom.2016.12.367.
[4] Y. Birol, Grain refining efficiency of Al–Ti–C alloys, J. Alloys. Compd. 422 (2006) 128–131, https://doi.org/10.1016/j.jallcom.2005.11.059.
[5] B.T. Gezer, F. Toptan, S. Daglilar, I. Kerti, Production of Al–Ti–C grain refiners with the addition of elemental carbon, Mater. Design. 31 (2010) S30–S35, https://doi.org/10.1016/j.matdes.2009.09.002.
[6] T.F. Ma, Z.Y. Chen, Z.R. Nie, H. Huang, Microstructure of Al-Ti-B-Er refiner and its grain refining performance, J. Rare Earth 31 (2013) 622–627, https://doi.org/10.1016/S1002-0721(12)60331-7.
[7] J.C. Dai, S.M. Zhu, M.A. Easton, W.F. Xu, G.H. Wu, W.J. Ding, Precipitation process in a Mg–Gd–Y alloy grain-refined by Al addition, Mater. Charact. 88 (2014) 7–14, https://doi.org/10.1016/j.matchar.2013.10.010.
[8] D. Du, J.C. Haley, A. Dong, Y. Fautrelle, D. Shu, G. Zhu, X. Li, B. Sun, E.J. Lavernia, Influence of static magnetic field on microstructure and mechanical behavior of selective laser melted AlSi10Mg alloy, Mater. Design 181 (2019) 107923, https://doi.org/10.1016/j.matdes.2019.107923.
[9] Y.D. Yu, C.X. Li, The effect of alternative low frequency electromagnetic field on the solidification microstructure and mechanical properties of ZK60 alloys, Mater. Design 44 (2013) 17–22, https://doi.org/10.1016/j.matdes.2012.07.034.
[10] R. Pongen, A.K. Birru, P. Parthiban, Study of microstructure and mechanical properties of A713 aluminium alloy having an addition of grain refiners Al-3.5 Ti-1.5C and Al-3Cobalt, Results. Phys. 13 (2019), 102105, https://doi.org/10.1016/j.rinp.2019.02.041.
[11] X. Xu, Y. Feng, H. Fan, Q. Wang, G. Dong, G. Li, Z. Zhang, Q. Liu, X. Fan, H. Ding, The grain refinement of 1070 alloy by different Al-Ti-B mater alloys and its influence on the electrical conductivity, Results. Phys. 14 (2019), 102482, https://doi.org/10.1016/j.rinp.2019.102482.
[12] T.S. Krishnan, P.K. Rajagopalan, B.R. Gund, J. Krishnan, D.K. Bose, Development of Al–5%Ti–1%B master alloy, J. Alloys. Compd. 269 (1998) 138–140, https://doi.org/10.1016/S0925-8388(98)00217-5.
[13] L. Li, Q. Zhu, H. Zhang, Y. Zuo, C. Ban, L. He, H. Liu, J. Cui, Morphological and crystallographic characterization of solidified Al–3Ti–1B master alloy under a high magnetic field, Mater. Charact. 95 (2014) 1–11, https://doi.org/10.1016/j.matchar.2014.05.022.
[14] Y. Wang, C.M. Fang, L. Zhou, T. Hashimoto, X. Zhou, Q.M. Ramasse, Z. Fan, Mechanism for Zr poisoning of Al-Ti-B based grain refiners, Acta. Mater. 164 (2019) 428–439, https://doi.org/10.1016/j.actamat.2018.10.056.
[15] Z. Fan, Y. Wang, Y. Zhang, T. Qin, X.R. Zhou, G.E. Thompson, T. Pennycook, T. Hashimoto, Grain refining mechanism in the Al/Al–Ti–B system, Acta. Mater. 84 (2015) 292–304, https://doi.org/10.1016/j.actamat.2014.10.055.
[16] H.D. Alamdari, D. Dubé, P. Tessier, Behavior of boron in molten aluminum and its grain refinement mechanism, Metall. Mater. Trans. A 44 (2013) 388–394, https://doi.org/10.1007/s11661-012-1388-x.
[17] D. Qiu, J.A. Taylor, M.X. Zhang, Understanding the Co-poisoning effect of Zr and Ti on the grain refinement of cast aluminum alloys, Metall. Mater. Trans. A 41A (2010) 3412–3420, https://doi.org/10.1007/s11661-010-0404-2.
[18] H. Jiang, Q. Sun, L. Zhang, J. Zhao, Al-Ti-C master alloy with nano-sized TiC particles dispersed in the matrix prepared by using carbon nanotubes as C source, J. Alloys. Compd. 748 (2018) 774–782, https://doi.org/10.1016/j.jallcom.2018.03.175.
[19] Y.C. Tzeng, S.Y. Jian, Effects of the addition of trace amounts of Sc on the microstructure and mechanical properties of Al-11.6Si alloys, Mater. Sci. Eng., A 723 (2018) 22–28, https://doi.org/10.1016/j.msea.2018.03.016.
[20] H. Zhao, Y. Song, M. Li, S. Guan, Grain refining efficiency and microstructure of Al–Ti–C–RE master alloy, J. Alloys. Compd. 508 (2010) 206–211, https://doi.org/10.1016/j.jallcom.2010.08.047.
[21] G.S. Vinod Kumar, B.S. Murty, M. Chakraborty, Development of Al–Ti–C grain refiners and study of their grain refining efficiency on Al and Al–7Si alloy, J. Alloys. Compd. 396 (2005) 143–150, https://doi.org/10.1016/j.jallcom.2004.12.039.
[22] A.R. Kennedy, A.E. Karantzalis, S.M. Wyatt, The microstructure and mechanical properties of TiC and TiB_2-reinforced cast metal matrix composites, J. Mater. Sci. 34 (1999) 933–940, https://doi.org/10.1023/A:1004519306186.
[23] N. Sobczak, J. Sobczak, S. Seal, J. Morgiel, TEM examination of the effect of titanium on the Al/C interface structure, Mater. Chem. Phys. 81 (2003) 319–322, https://doi.org/10.1016/S0254-0584(02)00592-8.
[24] P. Baumli, J. Sychev, I. Budai, J.T. Szabo, G. Kaptay, Fabrication of carbon fiber reinforced aluminum matrix composites via a titanium-ion containing flux, Composites: Part A 44 (2013) 47–50, https://doi.org/10.1016/j.compositesa.2012.08.021.
[25] A. Banerji, W. Reif, Metallographic investigation of TiC nucleants in the newly developed Al-Ti-C grain refiner, J. Mater. Sci. 29 (1994) 1958–1965, https://doi.org/10.1007/BF00351320.
[26] X.R. Chen, Y.H. Jia, Q.Y. Liao, W.T. Jia, Q.C. Le, S.C. Ning, F.X. Yu, The simultaneous application of variable frequency ultrasonic and low frequency electromagnetic fields in semi continuous casting of AZ80 magnesium alloy, J. Alloys. Compd. 774 (2019) 710–720, https://doi.org/10.1016/j.jallcom.2018.09.300.
[27] B. Nagasivamuni, G. Wang, D.H. StJohn, M.S. Dargusch, The effect of ultrasonic treatment on the mechanisms of grain formation in as-cast high purity zinc,

J. Cryst. Growth. 495 (2018) 20–28, https://doi.org/10.1016/j.jcrysgro.2018.05.006.
[28] X.R. Chen, F.K. Ning, J. Hou, Q.C. Le, Y. Tang, Dual-frequency ultrasonic treatment on microstructure and mechanical properties of ZK60 magnesium alloy, Ultrason. Sonochem. 40 (2018) 433–441, https://doi.org/10.1016/j.ultsonch.2017.07.027.
[29] X. Yang, S. Wu, S. Lu, L. Hao, X. Fang, Refinement of LPSO structure in Mg-Ni-Y alloys by ultrasonic treatment, Ultrason. Sonochem. 40 (2018) 472–479, https://doi.org/10.1016/j.ultsonch.2017.07.042.
[30] C.E.H. Tonry, G. Djambazov, A. Dybalska, W.D. Griffiths, C. Beckwith, V. Bojarevics, K.A. Pericleous, Acoustic resonance for contactless ultrasonic cavitation in alloy melts, Ultrason. Sonochem. 63 (2020) 104959, https://doi.org/10.1016/j.ultsonch.2020.104959.
[31] P. Madhukar, N. Selvaraj, R. Gujjala, C.S.P. Rao, Production of high performance AA7150-1% SiC nanocomposite by novel fabrication process of ultrasonication assisted stir casting, Ultrason. Sonochem. 58 (2019) 104665, https://doi.org/10.1016/j.ultsonch.2019.104665.
[32] H. Ye, K. Ye, B.-G. Guo, F.-B. Le, C. Wei, X. Sun, G.-Y. Wang, Y. Liu, Effects of combining ultrasonic micro-forging treatment with laser metal wire deposition on microstructural and mechanical properties in Ti–6Al–4V alloy, Mater. Charact. 162 (2020) 110187, https://doi.org/10.1016/j.matchar.2020.110187.
[33] Y. Zhao, D. Song, B. Lin, C. Zhang, D. Zheng, S. Inguva, T. Li, Z. Sun, Z. Wang, W. Zhang, 3D characterization of ultrasonic melt processing on the microstructural refinement of Al Cu alloys using synchrotron X-ray tomography, Mater. Charact. 153 (2019) 354–365, https://doi.org/10.1016/j.matchar.2019.04.040.
[34] G.S.B. Lebon, I. Tzanakis, K. Pericleous, D. Eskin, P.S. Grant, Ultrasonic liquid metal processing: the essential role of cavitation bubbles in controlling acoustic streaming, Ultrason. Sonochem. 55 (2019) 243–255, https://doi.org/10.1016/j.ultsonch.2019.01.021.
[35] G.S.B. Lebon, G. Salloum-Abou-Jaoude, D. Eskin, I. Tzanakis, K. Pericleous, P. Jarry, Numerical modelling of acoustic streaming during the ultrasonic melt treatment of direct-chill (DC) casting, Ultrason. Sonochem. 54 (2019) 171–182, https://doi.org/10.1016/j.ultsonch.2019.02.002.
[36] H. Puga, J. Barbosa, J.C. Teixeira, M. Prokic, A new approach to ultrasonic degassing to improve the mechanical properties of aluminum alloys, J. Mater. Eng. Perform. 23 (2014) 3736–3744, https://doi.org/10.1007/s11665-014-1133-2.
[37] G.I. Eskin, D.G. Eskin, Production of natural and synthesized aluminum-based composite materials with the aid of ultrasonic (cavitation) treatment of the melt, Ultrason. Sonochem. 10 (2003) 297–301, https://doi.org/10.1016/S1350-4177(02)00158-X.
[38] F. Wang, D. Eskin, J. Mi, T. Connolle, J. Lindsay, M. Mounib, A refining mechanism of primary Al3Ti intermetallic particles by ultrasonic treatment in the liquid state, Acta. Mater. 116 (2016) 354–363, https://doi.org/10.1016/j.actamat.2016.06.056.
[39] G. Wang, M.S. Dargusch, M. Qian, D.G. Eskin, D.H. StJohn, The role of ultrasonic treatment in refining the as-cast grain structure during the solidification of an Al–2Cu alloy, J. Cryst. Growth. 408 (2014) 119–124, https://doi.org/10.1016/j.jcrysgro.2014.09.018.
[40] M. Wang, Y. Zhao, L.D. Wang, Y.P. Zhu, X.J. Wang, J. Sheng, Z.Y. Yang, H.L. Shi, Z. D. Shi, W.D. Fei, Achieving high strength and ductility in graphene/magnesium composite via an *in-situ* reaction wetting process, Carbon 139 (2018) 954–963, https://doi.org/10.1016/j.carbon.2018.08.009.
[41] Z. Liu, Q. Han, J. Li, A developed method for producing in situ TiC/Al composites by using quick preheating treatment and ultrasonic vibration, Composites: Part B 43 (2012) 2429–2433, https://doi.org/10.1016/j.compositesb:2011.11.004.
[42] M.R. Dehnavi, B. Niroumand, F. Ashrafizadeh, P.K. Rohatgi, Effects of continuous and discontinuous ultrasonic treatments on mechanical properties and microstructural characteristics of cast Al413–SiCnp nanocomposite, Mater. Sci. Eng., A 617 (2014) 73–83, https://doi.org/10.1016/j.msea.2014.08.042.
[43] K.L. Juhasz, P. Baumli, J. Sytchev, G. Kaptay, Wettability of graphite by liquid aluminum under molten potassium halide fluxes, J. Mater. Sci. 48 (2013) 7679–7685, https://doi.org/10.1007/s10853-013-7586-0.
[44] V.H. López, A.R. Kennedy, Flux-assisted wetting and spreading of Al on TiC, J. Collold Interf. Sci. 298 (2006) 356–362, https://doi.org/10.1016/j.jcis.2005.12.040.
[45] N. Eustathopoulos, J.C. Joud, P. Desre, J.M. Hicter, The wetting of carbon by aluminium and aluminium alloys, J. Mater. Sci. 9 (1974) 1233–1242, https://doi.org/10.1007/BF00551836.
[46] D.A. Weirauch, W.M. Balaba, A.J. Perrotta, Kinetics of the reactive spreading of molten aluminum on ceramic surfaces, J. Mater. Res. 10 (1995) 640–650, https://doi.org/10.1557/JMR.1995.0640.
[47] P. Baumli, J. Sytchev, G. Kaptay, Perfect wettability of carbon by liquid aluminum achieved by a multifunctional flux, J. Mater. Sci. 45 (2010) 5177–5190, https://doi.org/10.1007/s10853-010-4555-8.
[48] K. Landry, S. Kalogeropoulou, N. Eustathopoulos, Wettability of carbon by aluminum and aluminum alloys, Mater. Sci. Eng., A 254 (1998) 99–111, https://doi.org/10.1016/S0921-5093(98)00759-X.
[49] T.V. Atamanenko, D.G. Eskin, M. Sluiter, L. Katgerman, On the mechanism of grain refinement in Al–Zr–Ti alloys, J. Alloys. Compd. 509 (2011) 57–60, https://doi.org/10.1016/j.jallcom.2010.09.046.
[50] J.R.G. Sander, B.W. Zeiger, K.S. Suslick, Sonocrystallization and sonofragmentation, Ultrason. Sonochem. 21 (2014) 1908–1915, https://doi.org/10.1016/j.ultsonch.2014.02.005.
[51] A. Straumal, I. Mazilkin, K. Tzoy, B. Straumal, K. Bryła, A. Baranchikov, G. Eggeler, Bulk and surface low temperature phase transitions in the Mg-alloy EZ33A, Metals 10 (2020), https://doi.org/10.3390/met10091127.
[52] B.B. Straumal, B. Baretzky, O.A. Kogtenkova, A.B. Straumal, A.S. Sidorenko, Wetting of grain boundaries in Al by the solid Al3Mg2 phase, J. Mater. Sci. 45 (2010) 2057–2061, https://doi.org/10.1007/s10853-009-4014-6.
[53] A.S. Gornakova, B.B. Straumal, A.N. Nekrasov, A. Kilmametov, N.S. Afonikova, Grain boundary wetting by a second solid phase in Ti-Fe alloys, J. Mater. Eng. Perform. 27 (2018) 4989–4992, https://doi.org/10.1007/s11665-018-3300-3.
[54] I. Mazilkin, K. Tsoy, A. Straumal, A. Rodin, B. Baretzky, Grain boundary wetting of different types of grain boundaries in the Cu–Ag system, Mater. Lett. 272 (2020), 127730, https://doi.org/10.1016/j.matlet.2020.127730.
[55] I. Konyashin, F. Lachmann, B. Ries, A.A. Mazilkin, B.B. Straumal, C. Kübel, L. Llanes, B. Baretzky, Strengthening zones in the Co matrix of WC–Co cemented carbides, Scripta Mater. 83 (2014) 17–20, https://doi.org/10.1016/j.scriptamat.2014.03.026.
[56] X. Kai, K. Tian, C. Wang, L. Jiao, G. Chen, Y. Zhao, Effects of ultrasonic vibration on the microstructure and tensile properties of the nano ZrB2/2024Al composites synthesized by direct melt reaction, J. Alloys. Compd. 668 (2016) 121-127. https://doi,org/10.1016/j.jallcom.2016.01.152.
[57] A.N. Guz, A.P. Zhuk, Motion of solid particles in a liquid under the action of an acoustic field: the mechanism of radiation pressure, Int. Appl. Mech. 40 (2004) 246-265. 10.1023/B:INAM.0000031907.28520.7b.
[58] S. Absar, P. Pasumarthi, H. Choi, Numerical and experimental studies about the effect of acoustic streaming on ultrasonic processing of metal matrix nanocomposites (MMNCs), J. Manuf. Process. 28 (2017) 515–522, https://doi.org/10.1016/j.jmapro.2017.04.020.
[59] Q. Lin, P. Shen, L. Yang, S. Jin, Q. Jiang, Wetting of TiC by molten Al at 1123–1323K, Acta Mater. 59 (2011) 1898–1911, https://doi.org/10.1016/j.actamat.2010.11.055.
[60] Y. Fang, T. Yamamoto, S. Komarov, Cavitation and acoustic streaming generated by different sonotrode tips, Ultrason. Sonochem. 48 (2018) 79–87, https://doi.org/10.1016/j.ultsonch.2018.05.011.